

Contrasting behaviour from two Be/X-ray binary pulsars: insights into differing neutron star accretion modes

L. J. Townsend,^{1*} S. P. Drave,¹ A. B. Hill,^{1,2} M. J. Coe,¹ R. H. D. Corbet,³
A. J. Bird¹ and M. P. E. Schurch⁴

¹Faculty of Physical and Applied Sciences, University of Southampton, Highfield, Southampton, SO17 1BJ, UK

²W. W. Hansen Experimental Physics Laboratory, Kavli Institute for Particle Astrophysics and Cosmology, Department of Physics and SLAC National Accelerator Laboratory, Stanford University, Stanford, CA 94305, USA

³University of Maryland Baltimore County, X-ray Astrophysics Laboratory, Mail Code 662; NASA Goddard Space Flight Center, Greenbelt, MD 20771, USA

⁴Astrophysics, Cosmology and Gravity Centre (ACGC), Astronomy Department, University of Cape Town, Rondebosch, Private Bag XI 7701, South Africa

Accepted 2013 April 15. Received 2013 April 4; in original form 2012 September 14

ABSTRACT

In this paper we present the identification of two periodic X-ray signals coming from the direction of the Small Magellanic Cloud (SMC). On detection with the *Rossi X-ray Timing Explorer* (*RXTE*), the 175.4 s and 85.4 s pulsations were considered to originate from new Be/X-ray binary (BeXRB) pulsars with unknown locations. Using rapid follow-up *INTEGRAL* and *XMM-Newton* observations, we show the first pulsar (designated SXP175) to be coincident with a candidate high-mass X-ray binary (HMXB) in the northern bar region of the SMC undergoing a small Type II outburst. The orbital period (87 d) and spectral class (B0-B0.5IIIe) of this system are determined and presented here for the first time. The second pulsar is shown not to be new at all, but is consistent with being SXP91.1 – a pulsar discovered at the very beginning of the 13 year long *RXTE* key monitoring programme of the SMC. Whilst it is theoretically possible for accreting neutron stars to change spin period so dramatically over such a short time, the X-ray and optical data available for this source suggest this spin-up is continuous during long phases of X-ray quiescence, where accretion-driven spin-up of the neutron star should be minimal.

Key words: stars: emission-line, Be – Magellanic Clouds – X-rays: binaries.

1 INTRODUCTION

High-mass X-ray binaries (HMXB) consist of a massive early-type main-sequence or supergiant star and a neutron star or black hole compact object. They are found in regions of high gas and dust, such as the spiral arms of the Milky Way. As such, they are excellent tracers of star formation and ideal objects through which to study star-forming galaxies. The main sub-groups of HMXBs are the Be/X-ray binaries (BeXRB) and supergiant X-ray binaries (SGXB), making up a large fraction of the known population. The newly emerging classes of supergiant fast X-ray transients (SFXT; e.g. Sguera et al. 2005; Sidoli 2011) and gamma-ray binaries (e.g. Hill et al. 2011) complete the HMXB family. The Galactic population includes all of the above classes of HMXB, as well as a mixture of neutron star and black hole compact objects. This is markedly different to the population in the Small Magellanic Cloud (SMC), which consists only of BeXRBs and one SGXB, all of which have a neutron star accretor. The number of HMXBs in the SMC is also at odds with what is known from observations of the Galaxy. A simple

mass comparison suggests there should be only one or two such systems in the SMC, and yet there are over 60 now known. Population synthesis models by Dray (2006) predict the low-metallicity environment in the SMC could increase the number of HMXBs by a factor of 3. However, this is still not sufficient to explain the SMC population on its own. A recent episode of star formation, possibly due to an increase in the tidal force exerted on the SMC by a close approach with the Large Magellanic Cloud (LMC; Gardiner & Noguchi 1996; Diaz & Bekki 2011), is the current favoured scenario to explain the number of HMXBs observed.

The most numerous of the HMXBs, the BeXRBs, are the subject of this paper. They consist of a neutron star and an early-type Be or late Oe main-sequence secondary star. The neutron star is usually in a wide, eccentric orbit allowing for long periods of little X-ray activity. Classically, X-ray outbursts from these systems fall into one of two types: Type I outbursts occur near periastron passage of the neutron star where there is more accretable material, last for a few days to a week and have luminosities around 10^{36} erg s⁻¹. Studying these outbursts allows orbital periods to be derived through timing analysis of their light curves. Type II outbursts are typically an order of magnitude brighter than Type I outbursts and can last much longer. The cause of this being an enlargement of the circumstellar

*E-mail: ljt203@soton.ac.uk

material or radially driven wind around the companion star (e.g. Negueruela & Okazaki 2000), allowing accretion to occur at any orbital phase and at a higher rate.

The SMC provides an excellent laboratory to study both the fundamental physics of individual BeXRB systems and the global properties of a substantial population formed at the same time and at a well-defined distance. The latter can give an insight into the star-forming history of the galaxy and improve our understanding of how differences in the local environment (e.g. metallicity) affect the formation and evolution of the binary system. The former allows us to observe the interaction between a compact object and a massive star and how the compact object behaves under varying levels of accretion. In turn, this can provide information about the fundamental properties of the compact object such as the neutron star equation of state or black hole masses. In this paper, we present X-ray and optical data of two BeXRB pulsars in the SMC during recent X-ray outbursts. The first is a previously undiscovered system, adding to the already vast population. We show that this system is typical of many others in the SMC. The second system, however, shows a constant spin-up of the neutron star during luminosity changes of several orders of magnitude. This characteristic has not been observed before and suggests that something unusual is happening to the accretion mode or near the emission region in this system. The X-ray and optical data are presented in Sections 2 and 3, respectively. We discuss the data and their implications in section 4 before concluding on our results in Section 5.

2 X-RAY OBSERVATIONS

2.1 SXP175 = RX J0101.8–7223

The *Rossi X-ray Timing Explorer (RXTE)* Proportional Counter Array (PCA) [see Jahoda et al. (2006) for instrument details and calibration model] detected 175.4 ± 0.1 s pulsations coming from the direction of the SMC on 2011 March 19 (MJD 55639) during an observation as part of a key programme to monitor X-ray binary activity in the SMC (Galache et al. 2008). The observation was made in the GoodXenon event mode and the data extracted using the standard reduction commands from `HEASOFT` v.6.9. The light curve was then binned at 0.01 s before being background subtracted and barycentre corrected. Finally, we corrected the count rate for the number of active Proportional Counter Units (PCUs). The final light curve was subjected to a Lomb–Scargle periodogram search for periodic changes in the flux. The error associated with any period found is calculated based on the formula given in Horne & Baliunas (1986). This period was confirmed by a second detection at 175.1 ± 0.1 s on 2011 March 26 (MJD 55646). It did not coincide with the spin period of any known pulsar in the *RXTE* field of view (FOV), and so was concluded to be a new HMXB pulsar in the SMC. The entire *RXTE* data archive was subsequently searched in order to build up an activity history of the pulsar (henceforth referred to as SXP175 under the naming convention of Coe et al. 2005). Unfortunately, this source has shown very little X-ray activity despite good coverage with the PCA over approximately 9 of the last 13 years. Only a handful of low significance ($<2\sigma$) detections are seen in the long-term light curve. These detections are sporadic and no orbital information could be drawn from the data.

An *INTEGRAL* (Winkler et al. 2003) ToO follow up observation was performed on 2011 April 2 (MJD 55653) to localize any X-ray sources within the *RXTE* FOV. The observation consisted of 50 individual Science Windows (ScW) summing to a total good time exposure of ~ 89.5 ks. Nominally, an ScW represents an ~ 2000 s

exposure. Both the hard IBIS/ISGRI (Lebrun et al. 2003; Ubertini et al. 2003) and soft JEM-X (Lund et al. 2003) X-ray data were analysed using the *INTEGRAL* Offline Science Analysis software (OSA v9.0; Goldwurm et al. 2003). Images were generated at ScW level in the 3–10 keV and 15–60 keV energy bands for JEM-X and IBIS, respectively, and combined into mosaics of the total observation. These mosaics are shown in Fig. 1 with the *RXTE*/PCA pulsation detection pointing overlaid. A single source is detected within the PCA FOV with a significance of 6.2σ in the IBIS revolution map, with a 90 per cent error circle on its position of radius 3.9 arcmin (Scaringi et al. 2010). The other fluctuations visible in the significance maps were not identified as real sources by the OSA source detection algorithms either because they are beneath the new source detection limit or their PSF is inconsistent with the known IBIS PSF which is well characterized at all positions within the FOV of the instrument. The detection limit was set at 4σ for a source at a position coincident with a known X-ray source and 6σ for a potential new source that is not coincident with a known X-ray source. As such, fluctuations that appear by eye to be of similar magnitude may be quite different. The source was not detected in the 3–10 keV energy band in the corresponding JEM-X map. The detection permitted an *XMM-Newton* ToO observation to identify the nature of the source.

An *XMM-Newton* observation was carried out on 2011 April 8 (MJD 55659) with the EPIC cameras in full frame, imaging mode. *XMM-Newton* has three X-ray telescopes (Aschenbach et al. 2002), one equipped with EPIC-pn (Strüder et al. 2001) and two with EPIC-MOS (Turner et al. 2001) CCD detectors in the focal plane. For data reduction we selected events with `PATTERN` ≤ 12 in a circular extraction region, placed on the source. Filtering of periods with high background was not necessary, since soft proton flares were at a quiescent level, yielding a net exposure time of 18.5 ks. A background region was chosen from a source-free region of the chip in which the source was seen, such that the RAWY positions were the same to minimize the background variation across each chip. Source detection and light-curve extraction were carried out using standard `SAS`¹ tools. A single bright X-ray source was found within the IBIS error circle at the position RA = 01:01:52.5, Dec. = $-72:23:34.9$ (J2000.0) with a 1σ error circle of radius 1.1 arcsec. A Lomb–Scargle periodogram of the 0.2–10 keV light curve revealed a period of 175.1 ± 0.1 s, confirming the *RXTE*, *INTEGRAL* and *XMM-Newton* detections are of the same source.

For spectral analysis we used only events with `PATTERN` ≤ 4 . The response matrices and ancillary files were created using the `SAS` tasks `RMFGEN` and `ARFGEN`. The X-ray spectrum was fitted with an absorbed power law with Galactic photoelectric absorption, N_{H} , fixed at $6 \times 10^{20} \text{ cm}^{-2}$ (Dickey & Lockman 1990) and the SMC column density, with abundances at 0.2 for metals, a free fit parameter (Fig. 2). This resulted in a photon index of 0.96 ± 0.02 and intrinsic SMC absorption of $(4.7 \pm 0.3) \times 10^{21} \text{ cm}^{-2}$. The full list of model parameters is presented in Table 1. The 0.2–10 keV flux from the fit is $8.5 \times 10^{-12} \text{ erg cm}^{-2} \text{ s}^{-1}$, corresponding to $3.7 \times 10^{36} \text{ erg s}^{-1}$ at the distance of the SMC (60 kpc; Hilditch et al. 2005). These spectral parameters are fairly standard for a BeXRB and suggest that the non-detection with JEM-X is more likely due to a low signal-to-noise ratio in the less sensitive of the two *INTEGRAL* instruments, rather than the hardness of the emission. The pulsar is coincident with the HMXB candidate RX J0101.8–7223 (Haberl & Sasaki 2000; Yokogawa et al. 2003) and is believed to

¹ Science Analysis Software (`SAS`), <http://xmm.esac.esa.int/sas/>

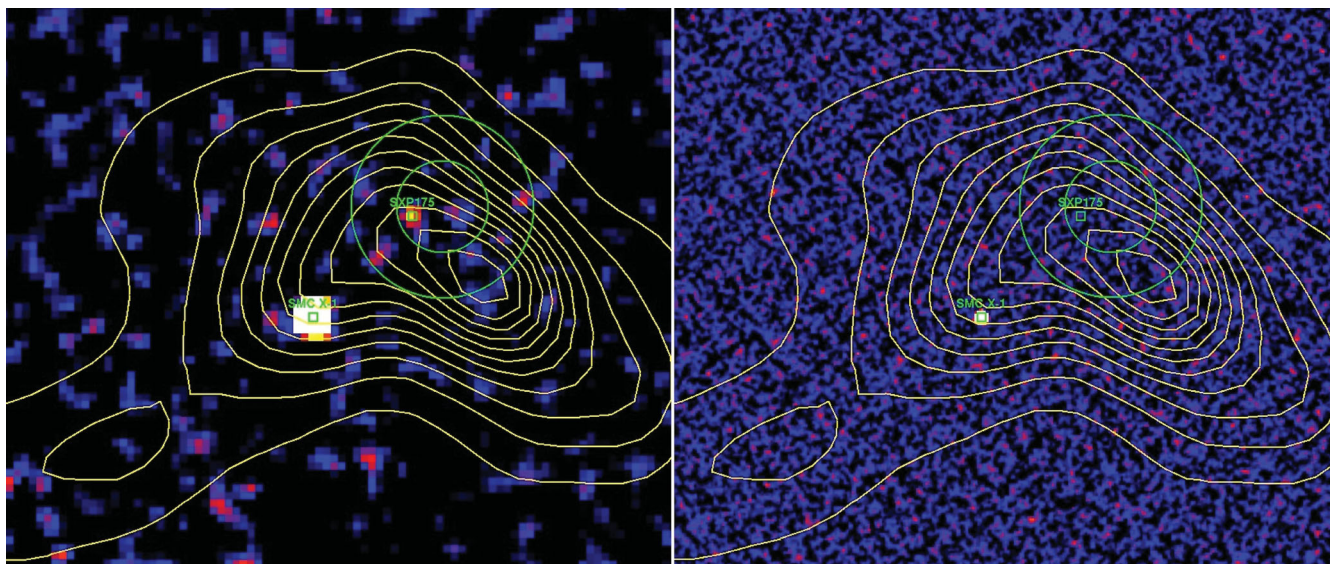


Figure 1. Left: *INTEGRAL*/IBIS 15–60 keV significance map of an observation performed on 2011 April 2 (MJD 55653). A single source is detected within the *RXTE*/PCA FOV at a significance of 6.2σ . The circles indicate the *RXTE*/PCA half and zero response of the pointing used whilst the contours are those of the H I column density of Putman et al. (2003). Right: *INTEGRAL*/JEM-X 3–10 keV significance map showing a non-detection at the location of the IBIS source.

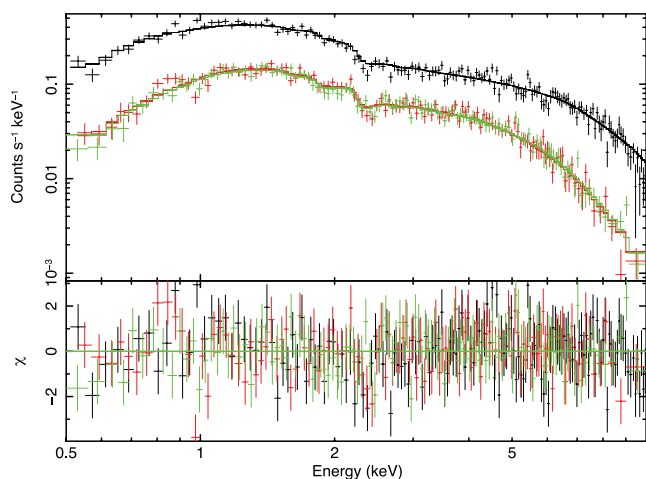


Figure 2. *XMM-Newton* EPIC spectra of SXP175. EPIC-PN is shown in black and EPIC-MOS in red (MOS1) and green (MOS2). The three spectra were fitted simultaneously with an absorbed power law allowing only a constant normalization factor between the three spectra. The model fit is presented in Table 1.

be the same object. The counterpart is likely the emission line star [MA93] 1288 (Meyssonnier & Azzopardi 1993). Optical and IR data of this star are explored in the next section.

2.2 SXP91.1 = AX J0051–722 = RX J0051.3–7216

SXP91.1 = AX J0051–722 = RX J0051.3–7216 was the first pulsar to be discovered in the *RXTE* monitoring programme at a period of 92 ± 1.5 s (Marshall, Lochner & Takeshima 1997). Further analysis refined this measurement to 91.12 ± 0.05 s (Corbet et al. 1998). The original positional uncertainty from the *ASCA* observation was 1.2 arcmin; however, this was later improved on by a *ROSAT* observation that yielded a position of RA = 00:50:59.3, Dec. = $-72:13:26$ (J2000.0) with a positional uncertainty of radius

Table 1. Results of absorbed power-law fits to EPIC spectra of SXP175 and SXP91.1.

Spectral parameter	SXP175	SXP91.1
Date	2011/04/08	2009/09/27
SMC N_{H} (10^{22} cm^{-2})	0.47 ± 0.03	6.55 ± 0.44
Photon index	0.96 ± 0.02	0.95 ± 0.06
χ^2_{ν} /degrees of freedom	1.08/391	1.13/158
Model flux ($10^{-12} \text{ erg cm}^{-2} \text{ s}^{-1}$) ^a	8.50 (M2)	1.92 (M2)
Luminosity ($10^{36} \text{ erg s}^{-1}$) ^b	3.65	0.82

^aThe median 0.2–10 keV flux from the three detectors is presented, with the detector indicated in brackets. M2 = MOS2. ^bThe 0.2–10 keV luminosity at a distance to the SMC of 60 kpc (Hilditch, Howarth & Harries 2005). Errors signify the 90 per cent confidence level.

2.6 arcsec (Sasaki, Haberl & Pietsch 2000). The source was regularly seen during the first 2 years of the programme (1998–9) and again briefly during the fifth year of the programme (2002). After that it was not detected again with any certainty for over 7 years despite good coverage with *RXTE* for most of this period.

RXTE observations performed on 2010 August 16 and 2010 August 21 showed the presence of pulsations with a period of 85.4 ± 0.1 s in their power spectra (Corbet et al. 2010). On seeing this pulsation, it was believed not to be consistent with any known pulsar in the SMC. The period is close to the second harmonic of the known pulsars SXP169 and SXP172, but neither appeared likely to be the source of the 85.4 s pulsations. Recent measurements of SXP169 have shown a spin-up trend that has produced a period significantly different from twice 85.4 s (e.g. Galache et al. 2008) and the detection times are not consistent with the known orbital period or ephemeris of SXP169. The collimator response to SXP172 in the pointed observation is of the order of 5 per cent, making this source unlikely to be the origin of the pulsations unless it was accreting close to the Eddington limit for a $1.4 M_{\odot}$ neutron star. In addition, we see no evidence for modulation near twice 85.4 s in the power spectra of the light curves, but the second harmonic of this period

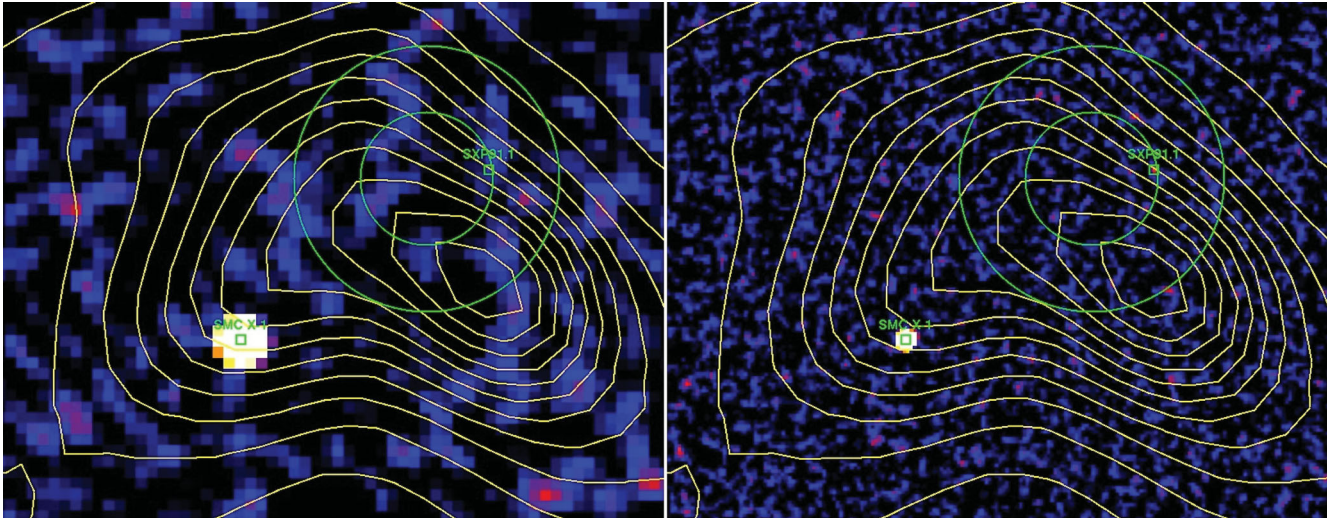


Figure 3. Left: *INTEGRAL*/IBIS 15–60 keV significance map of an observation performed on 2011 May 20 (MJD 55701). No significant sources are detected within the *RXTE*/PCA FOV. As before, the circles indicate the *RXTE*/PCA half and zero response of the pointing used whilst the contours are those of the H I column density of Putman et al. (2003). Right: *INTEGRAL*/JEM-X 3–10 keV significance map. The JEM-X source locator tool (`j_ima_src_locator`) identified a single source within the *RXTE*/PCA FOV detected at a significance of 5.6σ .

is present at 42.7 s. This pulsation was thus concluded to be from a new HMXB which was designated SXP85.4 (Corbet et al. 2010).

A Lomb–Scargle periodogram of the X-ray light curve allowed an epoch of maximum pulsed flux to be calculated. An orbital period of 88.42 ± 0.14 d (90 per cent confidence) is the best estimate derived from these X-ray data. From this ephemeris, the time of the next outburst was predicted to allow scheduling of an *INTEGRAL* follow-up observation to try and localize the X-ray pulses. An *INTEGRAL* ToO observation was carried out on 2011 May 20 (MJD 55701). The data were processed using the same methods and energy bands as the SXP175 observations. No sources were detected within the *RXTE*/PCA FOV by IBIS (Fig. 3, left). However, the JEM-X source locator tool (`j_ima_src_locator`) identified a clear source in the JEM-X combined mosaic at RA = 00:51:00, Dec. = $-72:14:20$ (2000) with a significance of 5.6σ and an uncertainty of 3 arcmin (Fig. 3, right). Along with SMC X–1, this was the only X-ray source identified by the source locator tool within the image. The position calculated from the JEM-X mosaic is completely consistent with that of SXP91.1. From this realization, we immediately combined the outburst histories of SXP85.4 and SXP91.1 in the figure caption. The errors on the spin period measurements are calculated as stated earlier and only detections of periodic modulation above a significance of 99 per cent are plotted for clarity reasons. The significance of each detection of a given frequency is related to its Lomb–Scargle power, P , by the following formula:

$$\text{significance} = 100 \times (1 - e^{-P})^M \quad (1)$$

where M is the number of independent frequencies and is typically 2×10^5 in our analysis pipeline. As can be seen, the spin period evolution of the recent episode of Type I outbursts is consistent with the evolution of the period between MJD 50800–51600. Along with the position determined by *INTEGRAL*, this is strong evidence that SXP85.4 is actually SXP91.1. Thus, this source will herein be discussed as SXP91.1. An even more intriguing observation is that SXP91.1 appears to be spinning up at a constant rate, through long periods of X-ray emission and through long periods of X-ray qui-

escence. This unexpected result could have significant implications for the accretion mode or the environment around the emission region in this system and is discussed in detail later in the paper. By analysing the data between MJD 55000–56000 we determine the orbital period and ephemeris of maximum amplitude of this system to be 87.80 ± 0.11 d and MJD 55429.0 ± 2.6 , respectively (90 per cent confidence). The reason for the small discrepancy between this value and that stated earlier (88.42 ± 0.14 d) is that the data were re-analysed to better remove the effect of a strong outburst from another pulsar in the power spectrum. This resulted in a spin period measurement being excluded from the more recent orbital period analysis as it was the product of a noisy power spectrum. A Lomb–Scargle analysis of the entire light curve reproduces these results at a lower level of significance. This is because the apparent Type II outburst around MJD 50800 and the sparseness of the observations during the early years of the programme detected fewer periodic outbursts than the most recent years of data. These results will be compared to those found from the analysis of SXP91.1s optical light curve and discussed further in the coming sections.

A search through the *XMM-Newton* archive showed two observations were previously made containing the position of SXP91.1 (observations 0301170201 and 0601210701), taken on MJD 53817.3 and 55101.7, respectively. A similar search of the *Chandra*, *ROSAT* and *Swift* archives did not return any useful observations. The latter of the two *XMM-Newton* observations was taken just before *RXTE* detected the 85.4 s pulsations, though no periodicities were found in the data. A spectrum was extracted for the PN and MOS2 detectors as described for SXP175 (the source was not inside the MOS1 detector FOV). These spectra were fit simultaneously with parameters fixed as described earlier and are shown in Fig. 5. This resulted in the list of model parameters presented in Table 1. The 0.2–10 keV flux from the fit is 1.9×10^{-12} erg cm $^{-2}$ s $^{-1}$, corresponding to 8.2×10^{35} erg s $^{-1}$ at the distance of the SMC. The source was not observed to be active in the other *XMM-Newton* observation. An upper limit for the flux was derived, corresponding to a limiting luminosity of $\sim 4 \times 10^{33}$ erg s $^{-1}$ (Haberl, private communication). This upper limit confirms that the source was indeed in deep quiescence during the period of non-detections with *RXTE*.

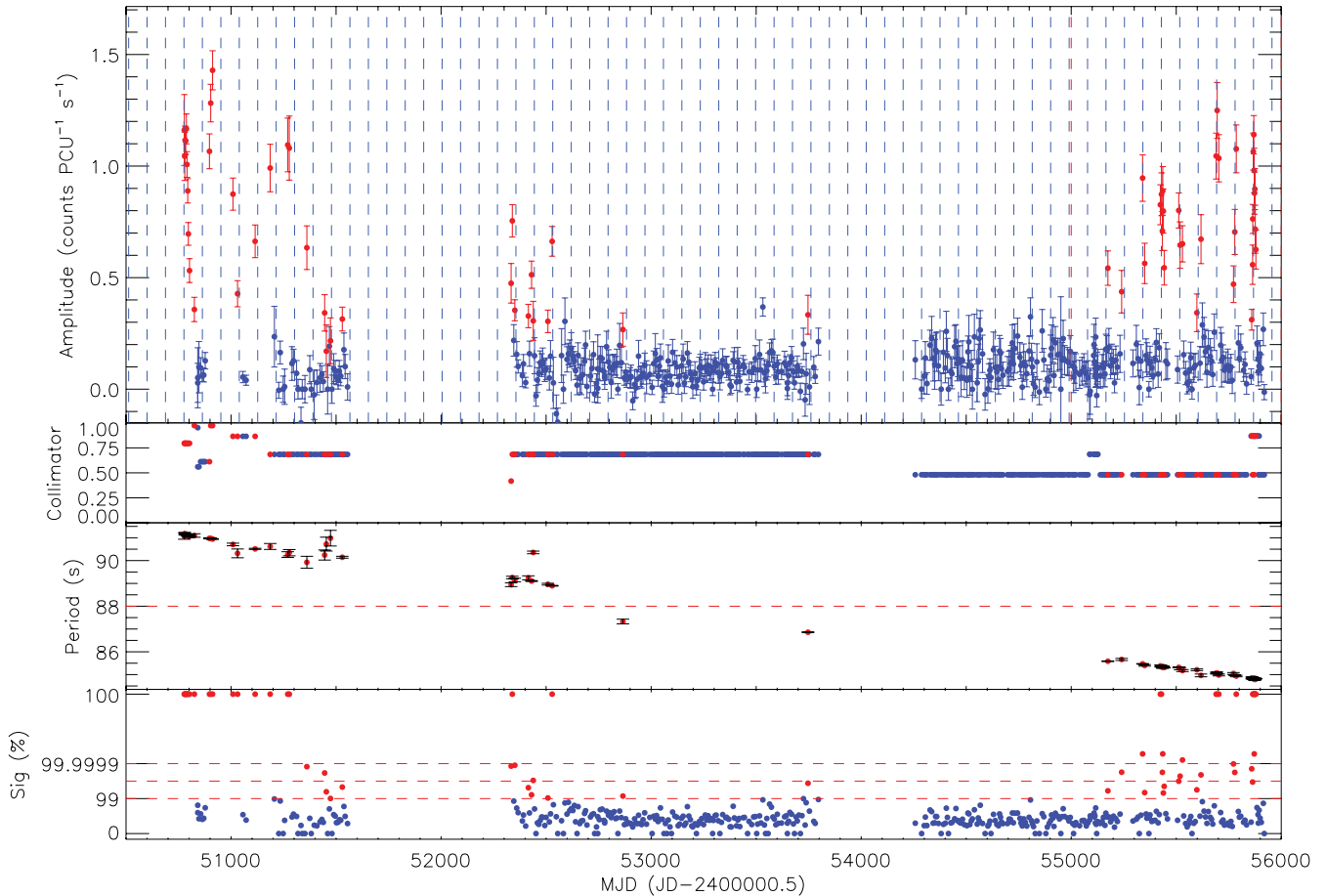


Figure 4. Long-term *RXTE*/PCA light curve of SXP91.1 in the 3–10 keV band. The top panel shows the amplitude of the pulsed emission, where each point is a single observation. The vertical blue dashed lines show the most likely X-ray ephemeris based on an orbital period search of the light curve. The second panel shows the source position within the *RXTE* FOV. A source at the very centre has a collimator response of 1 and a source at the very edge 0. The collimator response is approximately linear with distance from the centre. The third panel shows the pulse period measurements in seconds. The final panel shows the significance of the detection. The calculation of the significance is described in the text. Detections above a significance level of 99 per cent are plotted in red, with anything below this level plotted in blue. The source had good coverage with *RXTE* between MJD 52300–55000, though very few X-ray outbursts were detected. A constant spin-up can be fit to the entire spin period history, despite this apparent lack of accretion. This is discussed in greater detail in the text.

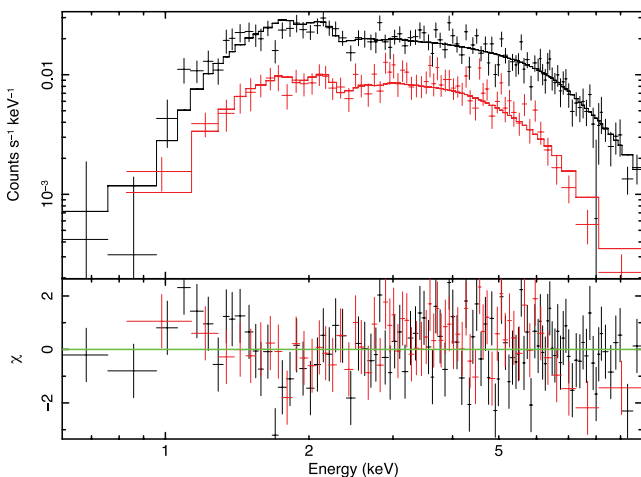


Figure 5. *XMM-Newton* EPIC spectra of SXP91.1. EPIC-PN is shown in black and EPIC-MOS2 in red. The two spectra were fitted simultaneously with an absorbed power law allowing only a constant normalization factor between the two spectra. The model fit is presented in Table 1.

These observations raise two important questions about the mode of accretion in this system: How has the neutron star spun up during such long periods of quiescence and why are pulsations not detected at a luminosity of $8.2 \times 10^{35} \text{ erg s}^{-1}$, typical of the Type I outburst luminosity of almost every other BeXRB system?

3 OPTICAL AND INFRARED OBSERVATIONS

In this section we present an optical light curve, near-IR fluxes and optical spectra of the optical counterpart to SXP175 with the aim of understanding more fully the circumstellar disc and its role in the X-ray outburst and to spectrally classify the optical counterpart. We also present an optical light curve and spectra of the counterpart to SXP91.1 to try and understand what role the stellar environment has played in producing the large variations in X-ray flux seen from this system during the last 14 years.

3.1 SXP175

Fig. 6 shows the combined MACHO *R*-band and OGLE (Optical Gravitational Lensing Experiment) *I*-band light curve of the optical counterpart to SXP175. The star is no. 1288 in the catalogue

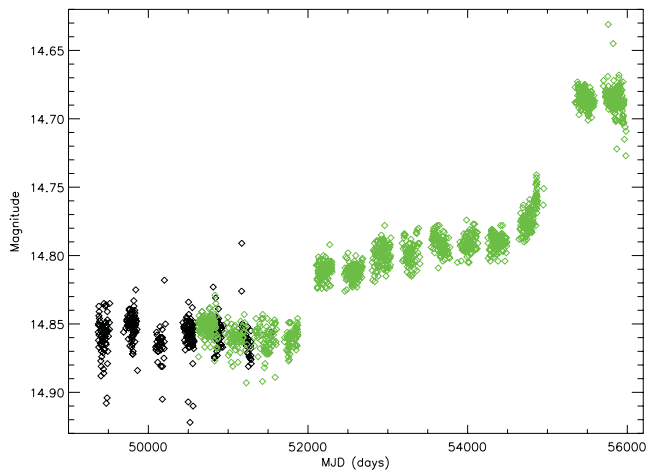


Figure 6. MACHO *R*-band (black points) and OGLE *I*-band (green points) light curve of the optical counterpart to SXP175. The MACHO data have been arbitrarily shifted to align roughly with the OGLE magnitude measurements at that time. The jumps at around MJD 52000 and MJD 55000 are the times at which the OGLE project moved from its second to third and third to fourth phases, respectively (OGLE II, III and IV). As such, we cannot be sure whether these increases in flux are real or whether they are a calibration effect.

Table 2. IRSF IR photometry of the counterpart to SXP175. The first measurement comes from Kato et al. (2007) using the same telescope and camera as the rest of the data.

Date (MJD)	<i>J</i>	<i>H</i>	<i>K_s</i>
2002-09-17 (52534)	14.82 ± 0.01	14.73 ± 0.02	14.53 ± 0.02
2007-12-18 (54452)	14.83 ± 0.01	14.67 ± 0.02	14.50 ± 0.03
2008-12-08 (54808)	14.82 ± 0.01	14.65 ± 0.01	14.47 ± 0.02
2009-12-14 (55179)	14.83 ± 0.02	14.65 ± 0.02	14.45 ± 0.05

of Meyssonier & Azzopardi (1993) and has the MACHO I.D. 207.16716.3 and OGLE II I.D. SMC-SC9 78833.² It shows very little periodic or long-term variability, besides a small increase in brightness around MJD 54800 by ~ 0.05 mag. At this time, there was good coverage of the source position with *RXTE*, though no X-ray activity was seen. This suggests the circumstellar disc had grown in the time between the end of the OGLE III light curve and the X-ray outburst. On three occasions near-infrared (NIR) data of the counterpart were obtained using the 1.4 m Infrared Survey Facility (IRSF) situated at the South African Astronomical Observatory (SAAO) to monitor the disc activity. The IRSF is a Japanese built telescope designed specifically to take simultaneous photometric data in the *J*, *H* & *K_s* bands with the SIRIUS (Simultaneous three-colour InfraRed Imager for Unbiased Survey) camera (Nagashima et al. 1999). Data reduction was performed using the dedicated SIRIUS pipeline.³ This performs the necessary dark subtraction, flat fielding, sky subtraction and recombines the dithered images, as well as producing a photometric catalogue of point sources in the reduced image. These data are presented in Table 2 and confirm the

² Light curves of objects associated with variable X-ray sources can be found in the OGLE real time monitoring of X-ray variables (XROM) programme. See <http://ogle.astrouw.edu.pl/ogle3/xrom/xrom.html> and Udalski (2008) for details.

³ <http://www.z.phys.nagoya-u.ac.jp/~nakajima/sirius/software/software.html>

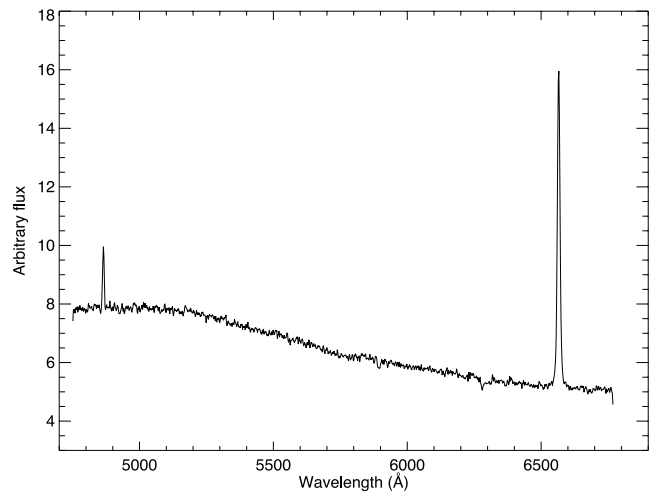


Figure 7. Optical spectrum of SXP175 taken with the ESO Faint Object Spectrograph and Camera (EFOSC) on the 3.6-m telescope at La Silla, Chile. *H α* and *H β* are observed to be in emission.

very stable nature of the disc over a long period of time. The only optical or NIR data taken closer to the X-ray outburst are the two years of OGLE IV data on the right of Fig. 6. As mentioned, the absolute calibration between the phases of the OGLE programme is uncertain and could vary by up to 0.2 mag. As such, we cannot put any trust in the leap of around 0.1 mag between phases III and IV. In fact, the brightening evident at the end of phase III is not obvious in phase IV, which is very flat and shows little sign of disc growth even though these data coincide with the X-ray outburst.

A red and blue spectrum of this source were taken from the European Southern Observatory (ESO) 3.6 m telescope at La Silla, Chile, on 2007 September 18 and 2007 September 19. The data were obtained with the ESO Faint Object Spectrograph (EFOSC2) mounted at the Nasmyth B focus of the 3.6-m New Technology Telescope (NTT), La Silla, Chile. The EFOSC2 detector (CCD 40) is a Loral/Lesser, Thinned, AR-coated, UV-flooded, MPP chip with 2048×2048 pixels corresponding to 4.1×4.1 arcmin² on the sky. The instrument was in longslit mode with a slit width of 1.5 arcsec. Grisms 14 and 20 were used for blue and red end spectroscopy, respectively. Grism 14 has a grating of 600 lines mm⁻¹ and a wavelength range of $\lambda\lambda 3095\text{--}5085$ Å producing a dispersion of 1 Å pixel⁻¹. The resulting spectra have a spectral resolution of ~ 12 Å. Grism 20 is one of the two new Volume-Phase Holographic grisms recently added to EFOSC2. It has 1070 lines pixel⁻¹ but a smaller wavelength range, from 6047 to 7147 Å. This results in a superior dispersion of 0.55 Å pixel⁻¹ and produces a spectral resolution for our red end spectra of ~ 6 Å. Filter OG530 was used to block second order effects. The data were reduced using the standard packages available in the Image Reduction and Analysis Facility (IRAF). Wavelength calibration was implemented using comparison spectra of Helium and Argon lamps taken through out the observing run with the same instrument configuration.

In the following section, we will use the blue spectrum to classify the star based in its absorption lines and their ratios. The red end spectrum is presented in Fig. 7, from which some important information can be gained. First, the presence of *H α* and *H β* lines in emission confirm the identification of this system as an emission-line XRB. The shape of both lines is very narrow and single peaked, suggesting the disc has a low inclination to our line of sight. Secondly, the equivalent widths of the lines can be

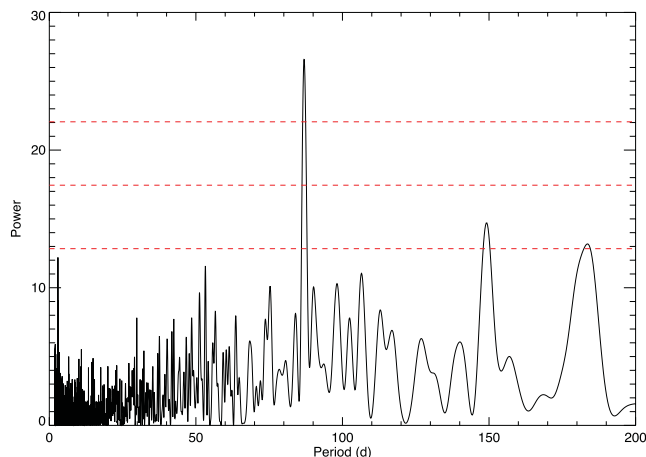


Figure 8. Power spectrum of the optical light curve of the counterpart to SXP175. Horizontal lines are 99 percent, 99.99 percent and 99.9999 percent confidence levels. The peak period is 86.9 ± 0.1 d.

measured. We estimate the equivalent width of the $H\alpha$ and $H\beta$ lines to be -25.7 \AA and -1.9 \AA , respectively. This value places the system nicely amongst other BeXRBs in the $H\alpha$ equivalent width against orbital period distribution (Reig, Fabregat & Coe 1997; Antoniou et al. 2009), and suggests the system should have an orbital period of approximately 90–100 d. This number is also implied from the Corbet diagram.

To this end, the light curve in Fig. 6 was detrended and searched for periodicities. The power spectrum is shown in Fig. 8. A peak at 86.9 ± 0.1 d is found at greater than the 99.9999 per cent confidence level. This seems likely to be the orbital period of the system, though until there is evidence of this period in the X-ray light curve, it cannot be certain that it is orbital in nature. Detrending was done with a simple third order polynomial. The peak found may move around slightly with a different detrending method, though it is safe to conclude the presence of a significant peak in the power spectrum at ~ 90 d that is likely the orbital period of the binary system.

3.1.1 Spectral classification

A star can be classified as emission line if $H\alpha$ (or any other hydrogen line usually seen in absorption in the hot, ionized photosphere) is filled in or is in emission, and so spectral coverage of the red part of the spectrum is vital. However, the spectral classification of emission line stars suffers many difficulties due to their very nature; the Balmer lines in particular will be rotationally broadened due to the high rotational velocities of Be stars and hence may obscure any comparisons to closely neighbouring lines, whilst the filling-in of lines caused by the disc emission also makes classification harder. Thus, it is beneficial to perform classification observations when the disc emission is minimal. Further difficulties arise when observing in the Magellanic Clouds. Classification of Galactic Be stars relies on using the ratio of many metal-helium lines (Walborn & Fitzpatrick 1990). However, this type of classification, based on the Morgan–Keenan (MK; Morgan, Keenan & Kellman 1943) system, is particularly difficult in the low-metallicity environment of the Magellanic Clouds because these metal lines are either very weak or not present at all. Using high signal-to-noise ratio spectra of SMC supergiants, Lennon (1997) devised a system for the classification of stars in the SMC that overcomes the problems with low-metallicity environments. This system is normalized to the MK

system such that stars in both systems exhibit the same trends in their line strengths. Thus, we have used the classification method as laid out in Lennon (1997) and utilized further in Evans et al. (2004). For the luminosity classification we adopted the classification method set out in Walborn & Fitzpatrick (1990).

The normalized and redshift-corrected spectrum used to spectrally classify SXP175 is presented in Fig. 9. The spectrum shows evidence of $\text{He II } \lambda 4686$ absorption, albeit fairly weak, meaning the star must be of type earlier than B 1 (Lennon 1997; Evans et al. 2004). Other ionized helium lines ($\text{He II } \lambda\lambda 4200, 4541$) may be present, but at a very weak level. This rules out a spectral type earlier than O 9.5. Given all of the He II lines are weak, we would suggest a B 0.5 class. However, if $\text{He II } \lambda\lambda 4200, 4541$ are present, the spectral type is more likely B 0. As it is difficult to confirm this above the noise in the continuum, we suggest a B 0–B 0.5 classification. As stated previously, the lack of strong metal lines makes the luminosity classification difficult. The $\text{He I } \lambda 4121/\text{He I } \lambda 4143$ ratio strengthens towards more luminous stars and is the only ratio that can be used here. The ratio in this spectrum is reasonably high, suggesting the luminosity class may be closer to III than V. A V-band magnitude of 14.6 (Haberl, Eger & Pietsch 2008) allows a check of this classification by comparing the absolute magnitude of the source with a distance modulus for the SMC of 18.9 (Harries, Hilditch & Howarth 2003). Thus, an absolute magnitude of -4.3 suggests (using absolute magnitudes for OeBe stars from Wegner 2006) a luminosity class of III, as a V–IV classification would suggest a spectral type as early as O 9. We suggest here a classification of B 0–B 0.5 IIIe is the most likely for this system given the information available. This is consistent with that of other BeXRBs in the SMC and in the Galaxy (e.g. McBride et al. 2008; Antoniou et al. 2009).

3.2 SXP91.1

Fig. 10 shows the combined MACHO R band and OGLE I-band light curve of the optical counterpart to SXP91.1. The star is no. 413 in the catalogue of Meyssonnier & Azzopardi (1993) and has the OGLE III I.D. SMC 102.1.32. It shows clear periodic variability, brightening by ~ 0.06 mag every 90 d, which is undoubtedly due to the orbital motion of the neutron star. A Lomb–Scargle analysis of the light curve reveals an extremely significant periodicity at 88.37 ± 0.03 d. The power spectrum is shown in Fig. 11. This period is consistent with that found from the analysis of the X-ray light curve and the period originally reported in Schmidtke et al. (2004) and is thus confirmed as the orbital period. There is very little long-term variability, besides a small increase in brightness between MJD 52800 and 53800 by ~ 0.05 mag. We note that the second of the 2 years of OGLE IV data is slightly fainter than the first, suggesting a slight shrinking of the disc during the X-ray outbursting phase. What is more interesting to note here, however, is that at the time of maximum optical flux in the OGLE III part of the light curve (MJD 53000–53500) there is no X-ray emission detected from this source. However, in the years preceding this small increase in optical flux, when the system appears to be in a constant low state, there were three consecutive Type I X-ray outbursts recorded in the *RXTE* monitoring data (MJD 52300–52600). This suggests X-ray emission only occurs, or at least only reaches the observer, at times of optical minima. This could mean that when the disc is larger, it is blocking most of the X-ray emission from the neutron star. This possibility is discussed in detail later. Even in the low state, X-ray emission is not always seen as is evident from the lack of X-ray activity between MJD 54000–55000. Similar NIR photometric measurements to those described earlier were taken using the IRSF

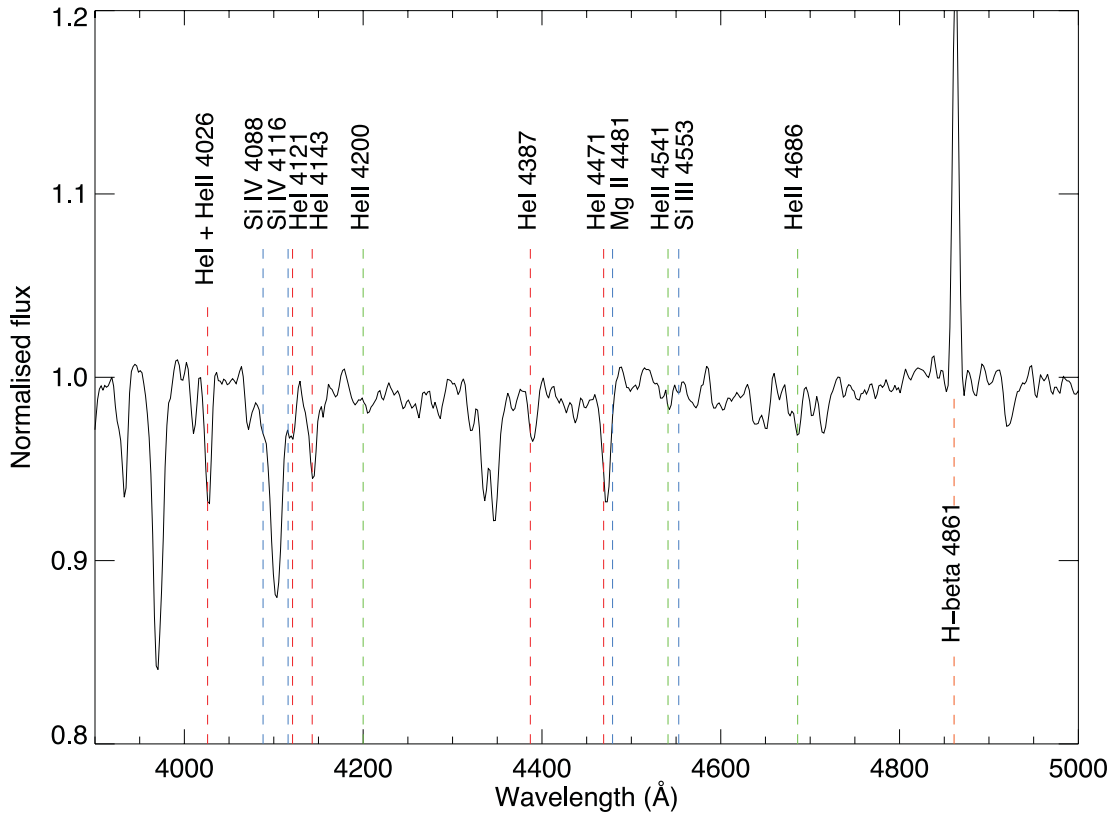


Figure 9. Spectrum of SXP175 taken with the EFOSC spectrograph on the 3.6-m telescope at La Silla, Chile. The spectrum has been normalized to remove the continuum and the data have been redshift corrected by -150 km s^{-1} to account for the recession of the SMC. Overplotted are various atomic transitions that are significant in the spectral classification of an early-type star at their rest wavelengths; He II, He I and metal transitions are in green, red and blue, respectively.

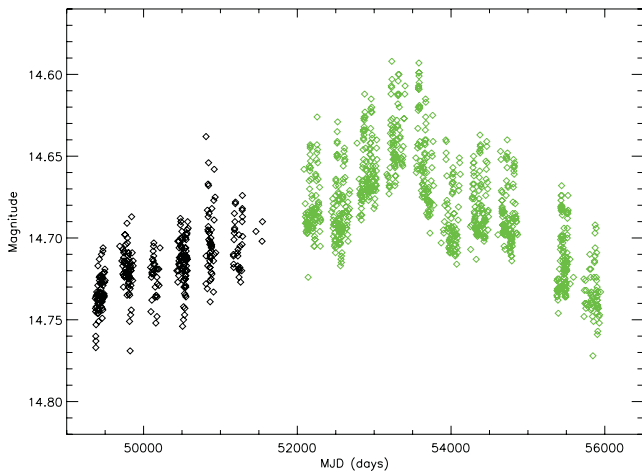


Figure 10. MACHO *R*-band (black points) and OGLE *I*-band (green points) light curve of the optical counterpart to SXP91.1. The MACHO data have been arbitrarily shifted to align roughly with the OGLE magnitude measurements at that time.

telescope at SAAO. These *J*, *H* and *K* images were taken on MJD 55179 and allowed for a measurement of the magnitude of the source in these bands. Values of $J = 14.776 \pm 0.011$, $H = 14.554 \pm 0.012$ and $K = 14.346 \pm 0.026$ suggest the disc is in a similar state to the last 3 years of the OGLE III light curve and consistent with the OGLE IV data. This implies that no dramatic change in the circumstellar environment induced the current long series of X-ray

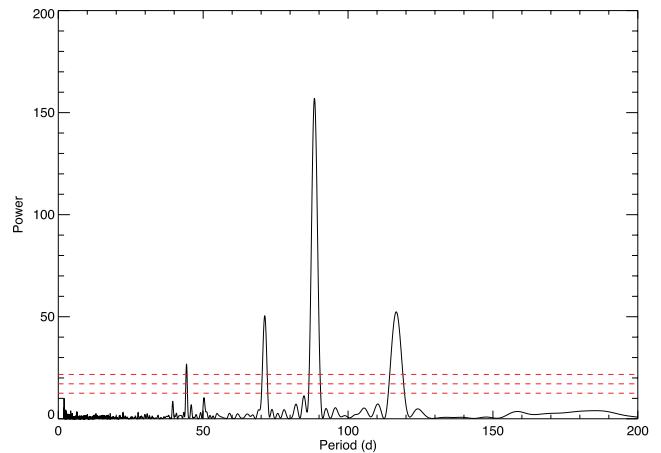


Figure 11. Power spectrum of the optical light curve of SXP91.1. Horizontal lines are 99 per cent, 99.99 per cent and 99.9999 per cent confidence levels. The peak period is $88.37 \pm 0.03 \text{ d}$. The second harmonic is visible at 44.2 d. The other peaks are likely to be aliasing caused by the data gaps in the OGLE light curve.

outbursts. Several $H\alpha$ spectra were also taken during this time period and are shown in Fig. 12. The first five of the seven spectra presented show almost constant equivalent widths (W_{eq}) of the $H\alpha$ line, with an average of -21.0 \AA and range between -20.2 and -21.4 \AA . Errors on these measurements are between 0.7 and 1.1 \AA . These spectra cover the time period of the OGLE light curve, reinforcing the idea of a very stable disc. The sixth and seventh spectrum,

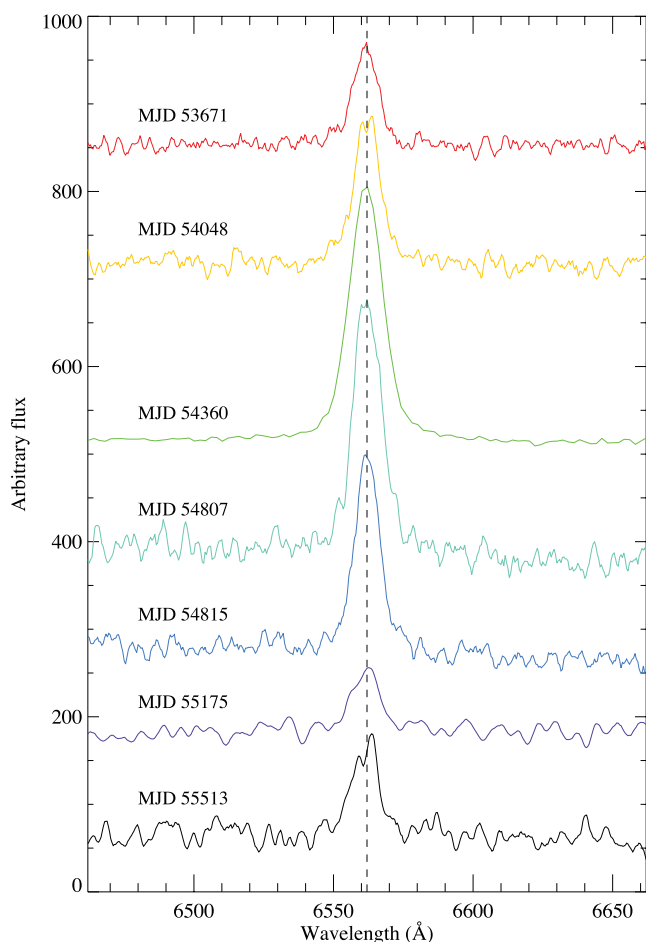


Figure 12. Optical spectra of SXP91.1 taken on the 1.9 m telescope at SAAO except the spectrum dated MJD 54360 which was taken on the 3.6 m telescope at La Silla. The vertical line denotes the rest wavelength of H α . All spectra have been arbitrarily shifted in flux and smoothed with a boxcar average of 5 Å width for viewing purposes.

however, show equivalent widths of -17.2 ± 1.6 and -27.3 ± 1.2 Å, respectively. Both were taken after the end of the OGLE light curve, suggesting there may have been some variability in the disc emission after this time. The full *RXTE* light curve for this source is presented in the next section where the discussion of these observations is continued.

4 DISCUSSION

The utilization of *INTEGRAL* and *XMM-Newton* to follow up on unidentified *RXTE* pulsars has proven to be very successful. In the preceding sections, we have discussed the discovery and localization of a new SMC pulsar (SXP175) to the HMXB candidate RX J0101.8–7223 and the association of a suspected new pulsar with an already known one (SXP91.1). The cause of the X-ray outburst from SXP175, which is the largest known from this HMXB, is not clear as the state of the disc at the time of the outburst is not known. It is likely that the disc increased in size, causing a small outburst. Previous observations of the region by *XMM-Newton* resulted in a positive detection of the source on five occasions, each time being at a flux level approximately 10 per cent of that detected in the ToO observation presented here (Haberl, private communication). This not only explains why it has never been seen with

RXTE at a significant level before, but also reinforces the idea that the disc may have grown and induced an outburst. The most recent of the aforementioned *XMM-Newton* detections was analysed by Haberl et al. (2008). They present a power-law fit to the spectrum that yields a photon index and intrinsic SMC absorption that are almost identical to those values presented here, despite the flux being <11 per cent of the flux measured in outburst. This shows that there was no change in the accretion column or surrounding material during the transition into outburst.

The analysis of data on SXP91.1 has shown that this particular BeXRB is quite abnormal from the rest of the population. The following accounts a short summary of the key observations made before potential explanations are given for the peculiar behaviour of the pulsar:

- (i) it has a high intrinsic absorption column of $(6.55 \pm 0.44) \times 10^{22} \text{ cm}^{-2}$.
- (ii) it was shown to be emitting unpulsed X-ray emission at a luminosity comparable to a Type I outburst ($8.2 \times 10^{35} \text{ erg s}^{-1}$) only one or two orbits before the first detection of pulsations with *RXTE*.
- (iii) it must have become much softer between the *XMM-Newton* detection and the *INTEGRAL* detection to be seen in JEM-X and not IBIS. This could mean it is softer in outburst (pulsed emission) but harder just before an outburst or at a slightly lower flux level (unpulsed emission).
- (iv) the long-term light curve suggests a constant spin-up under phases of outburst and quiescence. Quiescence is verified by the *XMM-Newton* non-detection with limiting luminosity of $\sim 4 \times 10^{33} \text{ erg s}^{-1}$.
- (v) its outbursting state seems not to be dependent on a change in the circumstellar disc. X-ray emission is both detected and not detected, when the optical flux (hence disc size) is unchanged. If anything, the X-ray outbursts are seen at the lowest optical flux level. If the state of the disc does not change and the orbital parameters do not change, then there is nothing to cause accretion to start or stop. This may mean there is always X-ray emission but, for some reason, this does not always reach the observer.

The *XMM-Newton* observation on MJD 55101 falls 0.2 of an orbital phase after periastron. Comparing this to the *RXTE* folded light curve (see Fig. 13) suggests this lies very close to the point at which pulsed emission ceases to be detected by *RXTE*. This limit is known to be around $10^{36} \text{ erg s}^{-1}$ in the SMC, which makes sense when the *XMM-Newton* derived luminosity is considered. The *RXTE* observation near MJD 55240 is the first confirmed detection of the source at a luminosity of $6 \times 10^{36} \text{ erg s}^{-1}$. Thus it seems that pulsed X-ray emission may only begin between luminosities of $(0.8\text{--}6) \times 10^{36} \text{ erg s}^{-1}$. From the theory of magnetospheric accretion (e.g. Corbet 1996), it is highly unlikely that this lack of pulsations at such a high luminosity is due to material not making its way to the neutron star surface. More likely, it is due to changes in the absorbing material around the system or changes in the hardness of the X-ray emission. Spectral fits to the few *RXTE* observations in which no other pulsar was active seem to suggest a softer power law than the *XMM-Newton* observation. This makes the later *INTEGRAL* detection with JEM-X more understandable as the source may have softened beyond what is detectable with IBIS, but it still does not explain why *XMM-Newton* did not see pulsations with sufficient counts and a normal value for the photon index. Another explanation is an energy dependence of the pulsed profile. Since the *RXTE* and *XMM-Newton* light curves were extracted in almost the same energy ranges, the pulsed fraction must

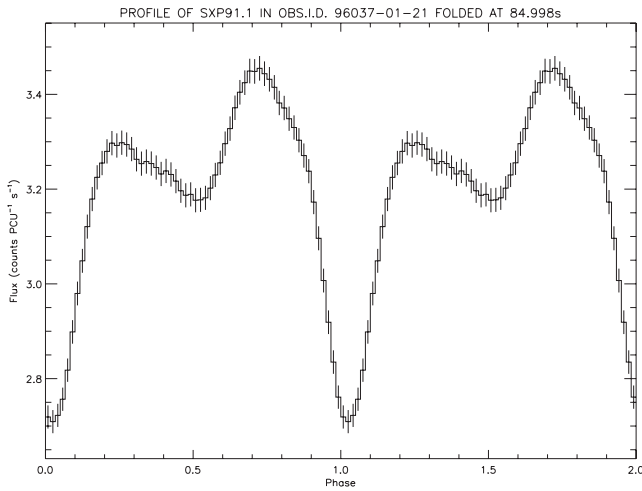


Figure 13. Example pulsed profile of SXP91.1 in the 3–10 keV band, folded at the detected spin period. The profile has been arbitrarily shifted in phase for viewing purposes.

have increased at softer energies between the *XMM-Newton* and *RXTE* detections. However, since energies much above 10 keV cannot be probed with *XMM*, this possibility is not testable. There was marginal evidence for variability in the H I column density between the *XMM-Newton* and *RXTE* observations, though this parameter was much less well constrained in the fits than the photon index and so drawing conclusions from this is not desirable.

The *RXTE* pulsed profiles were studied to investigate variability in the pulsed fraction and shape throughout the series of outbursts. The profile shown in Fig. 13 is representative of most of the profiles available. The pulsed shape is always double or triple peaked causing the presence of multiple harmonics in the power spectrum, with substantial variability in the relative strengths of the peaks. The pulsed fraction is approximately constant between outbursts, between 0.1 and 0.2, but shows a strong correlation with pulsed flux (and hence time) during individual outbursts. This may suggest an almost constant unpulsed component and that the pulsed component is much more variable under changing accretion rates. Again, it is hard to quantify the level of background emission in *RXTE* data, so these pulsed fractions are lower limits. To assess the non-pulsed detection of SXP91.1 during *XMM* observation 0601210701 we constructed a number of simulated light curves based upon the actual *XMM* light curve. A sinusoidal modulation with period 85.4 s was constructed with same sampling of the *XMM* light curve; this was then combined with the actual X-ray flux measurement such that the average flux remained the same and that a specific pulse fraction (PF) was achieved: $PF = \frac{F_{\max} - F_{\min}}{F_{\max} + F_{\min}}$. Each flux value is then shifted based upon the original error bar and assuming Gaussian errors. 2000 light curves were simulated for each PF over a range of 0.00–0.25 in steps of 0.01. The Lomb–Scargle periodogram was calculated for each light curve and all those corresponding to a given PF were averaged. To detect a signal in the data with a significance of $>5\sigma$ would require a PF of >14.8 per cent and at $>3\sigma$ would require a PF of >11.1 per cent. Our simulation ties in nicely with the *RXTE* observations, in that it shows the pulsed fraction of the source must have increased from below around 10 per cent prior to the *RXTE* observations, to above this value during the observations, allowing for the spin period detections.

Figs 14 and 15 show the folded orbital X-ray and optical light curves, respectively. Both show a broad profile not in-keeping with the fast-rise, exponential decay shape that is usually present in ec-

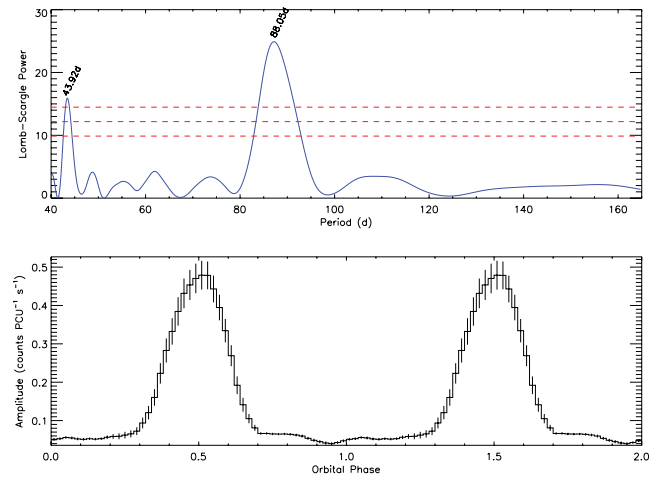


Figure 14. Top: orbital power spectrum of the long-term X-ray light curve of SXP91.1. The peak at 88.1 d signifies the orbital period of the system and agrees well with the optically derived period. The horizontal lines are 99 per cent, 99.99 per cent and 99.9999 per cent significances. Bottom: the X-ray light curve folded on the orbital period. The ephemeris of maximum amplitude is MJD 55516.43 ± 2.64 . Increased flux is apparent over a phase space of 0.4, higher than most other BeXRBs.

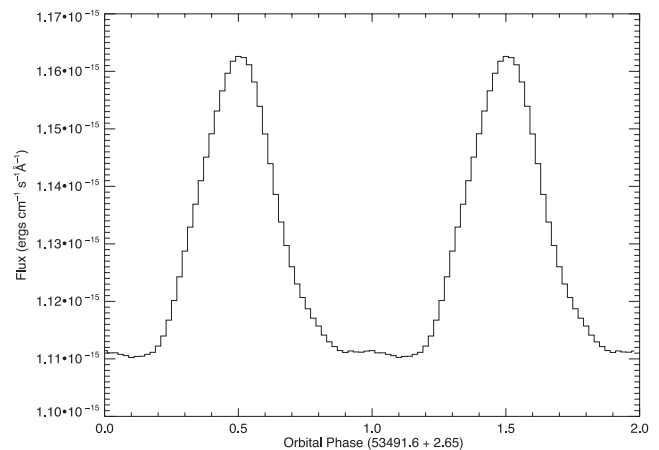


Figure 15. Folded optical light curve of SXP91.1. As with the X-ray light curve, a broad peak is observed suggesting the disturbance in the disc lasts for almost half an orbit.

centric accreting binaries. This broad emission region, spanning around half an orbital period, is indirect evidence of a low eccentricity in this system as the neutron star is accreting far beyond periastron. If true, this observation places SXP91.1 into a minority group amongst BeXRB pulsars. This may also help to explain the unusual spin-up that is observed through phases of quiescence in this system. If the orbit is near-circular, it could be accreting at a very low level all the time, spinning the neutron star up, whilst only becoming an X-ray pulsar when the accretion rate increases. However, as mentioned earlier, the cause of such an increase is hard to understand given the stability of the circumstellar disc. The optically and X-ray derived ephemerides agree well, with a suggestion that the peak in optical flux may lag the X-ray peak by no more than 6 d. The errors are large, however, so this value could be much less. Should the lag be real (5–10 per cent of an orbital period), it reinforces what is currently thought to occur during periastron

passage; that the disc only begins to be disturbed after the neutron star passes periastron (Jones et al., in preparation).

The constant state of the circumstellar disc is unusual during such a dramatic change in X-ray activity. NIR fluxes suggest that the constant nature of the disc seen in the OGLE light curve has continued well into the current X-ray active phase as discussed above. $H\alpha$ spectra taken before and during the X-ray active phase (see Fig. 12) shed some light on the problem, but also raise some further issues. The $H\alpha$ equivalent width measurement on MJD 55175 suggests a small decrease in the disc emission at the onset of the X-ray outburst, whilst the following measurement is evidence of a significant increase in the disc emission. At first, this may appear as evidence for the growth of the disc many hundreds of days into the series of X-ray outbursts. However, on closer inspection this observation falls nearly 2 weeks before periastron and so could just have been induced by the interacting neutron star rather than being an intrinsic change in the disc. A counter argument to this though is that four of the other spectra were taken as close or closer to periastron than this one and show no signs of an increase in flux. If the flux increase is intrinsic to the disc, it could indicate a significant lag between the start of the X-ray outburst and increased optical activity. Beyond this variability, these $H\alpha$ spectra show a further intriguing feature: the flux and shape of the profiles may correlate with orbital phase. The three profiles with the smallest W_{eq} were taken within a few days of periastron, whilst the three with the largest W_{eq} were taken at least 2 weeks before or after periastron. This could be evidence of the neutron star truncating the disc slightly (Negueruela & Okazaki 2001), though the reason for the changing profile shapes and their orbital phase distribution is very hard to understand with the data available.

4.1 Investigating the spin-up of SXP91.1

To explore the apparent spin-up of SXP91.1 we assessed the characteristics and data quality of each of the *RXTE* observations. The data set was filtered to include only observations where a periodic signal between 85 and 95 s was detected at a significance of >99.99 per cent and which had a collimator response of >0.4 . One additional data point was excluded as clearly being an outlier with a ~ 84 s period at early epochs. This left 37 *RXTE* observations of SXP91.1 where a periodic signal was detected. Errors on the periods were initially calculated using the analytical equations of Horne & Baliunas (1986). However, this method relies on well-behaved, high-quality data (e.g. the data show simple white noise). As the strength of the source signal varies significantly between observations we independently assessed the period errors for the Lomb–Scargle technique using a bootstrap method (see e.g. Kawano & Higuchi 1995).

For each of the filtered observations a simulated light curve is generated by a *bootstrap with replacement* technique which randomly selects a subset of ~ 68 per cent of the original light-curve points. The corresponding Lomb–Scargle periodogram is calculated and the period of the peak of highest power is recorded; this is repeated 200 000 times. To protect against extreme outliers in the simulations periods more than 3σ away from the median of the simulated periods are excluded; the standard deviation of the filtered sample of simulations is then taken as an estimate of the error.

In all except two of the observations, the bootstrap error was comparable to or greater than the errors from Horne & Baliunas (1986) and so to be conservative were adopted for the spin-up analysis. The remaining two observations were during a bright outburst and the bootstrap re-sampling did not yield distribution of periods with a finite width and hence for these two observations we adopt

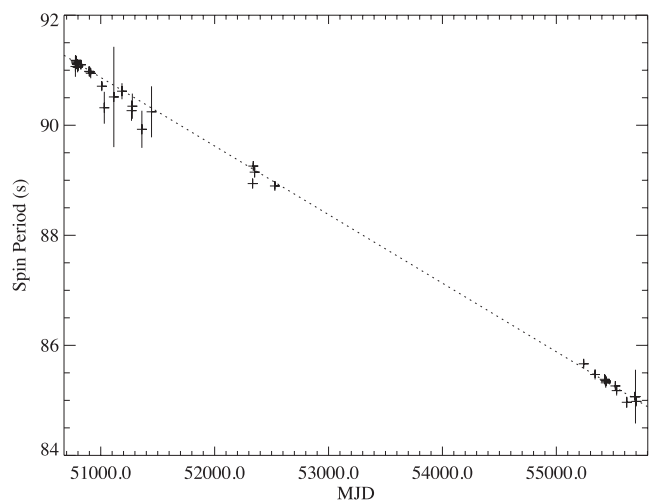


Figure 16. The fitted linear spin-up model of SXP91.1 is plotted as a dashed line over the *RXTE* spin-period detections. The individual *RXTE* period measurements are plotted with 1σ errors derived from bootstrapping the original data set (see text for details).

the analytical errors. The observations span ~ 13.5 yr, applying a simple linear spin-up model over all observations of:

$$P(t) = P(t_0) + \dot{P}(t - t_0) \quad (2)$$

yields a good-quality fit to the data with $\chi^2/\text{dof} = 41.2/35 = 1.18$ and giving a spin-up, $\dot{P} = 1.442 \pm 0.005 \times 10^{-8} \text{ s s}^{-1}$. We attempted to incorporate the orbital modulation of the pulsar into the spin-up model; however the sampling and quality of the data were not sufficient to constrain fitting a model of this type and consequently the simple linear spin-up model was found to be the best representation of the data. The data points with the bootstrap errors and best-fitting linear model are shown in Fig. 16.

Using this measurement, the average X-ray luminosity can be estimated assuming a given neutron star mass and magnetic moment, and assuming a constant accretion rate throughout our 13 years of observations. This final assumption is not unreasonable given the good fit to the spin periods presented above. Using the accretion models of Ghosh & Lamb (1979) whereby the compact object accretes from a disc, the spin-up and spin period measurements give an average luminosity of $(1.9 \pm 0.2) \times 10^{37} \text{ erg s}^{-1}$. This is markedly different from the $8.2 \times 10^{35} \text{ erg s}^{-1}$ calculated from the *XMM-Newton* spectrum shown earlier and hints at two or three possible explanations: first, the X-rays produced by the neutron star are in the region of $10^{37} \text{ erg s}^{-1}$ predicted by the model, but this light has been attenuated by an absorbing material around the neutron star or the binary system. Secondly, our interpretation of a constant accretion rate and spin up is correct, and the over-estimated average luminosity is due to our assumption of the mass or magnetic moment of the neutron star. In this case the mass of the neutron star would be less than the $1.4 M_{\odot}$ assumed or the magnetic moment would have to be higher than the $4.8 \times 10^{29} \text{ G cm}^3$ assumed. For completeness, we have calculated the possible extreme values of B and M assuming the observed average luminosity as an input into the accretion model. When calculating B, we used the observed L, P and \dot{P} and assumed a radius and mass of 10^6 cm and $1.4 M_{\odot}$, respectively. When calculating M, we assumed the above values and a magnetic moment of $4.8 \times 10^{29} \text{ G cm}^3$. The derived value of the magnetic field is $(3.1 \pm 0.1) \times 10^{13} \text{ G}$, consistent with a higher field than assumed

in our luminosity calculation. The value of M was not constrained by this calculation, suggesting that the low assumed magnetic field is indeed impossible for this observed luminosity. A third and final possibility is that our constant spin-up assumption could be incorrect and the neutron star has undergone varying levels of interaction with the Be star disc resulting in a variable luminosity. The latter scenario seems less likely given the evidence we have seen from the spin-up fit and the optical light curves. Thus, it is more likely that either the neutron star in this system has a larger magnetic field than average, or there is a variable absorbing material around the neutron star. There is strong evidence that such a variable absorber exists as it seems the only way to produce the variability seen in the X-rays without changing the accretion rate and, hence, the spin up of the neutron star. A potential such absorber may be a disc that absorbs the X-ray emission at certain times, possibly when it is enlarged.

5 CONCLUSIONS

This paper has presented the discovery of a new 175 s pulsar in the SMC and its association with the HMXB candidate RX J0101.8–7223. This system seems to be a very standard BeXRB system that has shown low levels of X-ray activity fairly regularly and a rare larger outburst that allowed the pulse period to be found. The large outburst is likely caused by an increase in the size of the circumstellar disc around the counterpart that, until now, has been very stable. An analysis of the optical light curve allowed an estimate of the orbital period of the system of 87.2 ± 0.2 d. An archival spectrum has allowed the counterpart to be classified as a B 0–B 0.5 IIIe star, similar to most other known BeXRBs.

SXP91.1 has proven to be very different to SXP175, with very regular outbursts, large modulation in its optical light curve and peculiar spin-up and X-ray emission characteristics. We have endeavoured to explain these aspects by combining all available X-ray, optical and IR data. It seems clear that the neutron star has always and is continuing to interact with the circumstellar disc at every periastron passage from the periodic variations in the OGLE light curve, though this interaction does not always lead to observable X-ray emission, pulsed or otherwise, reaching the observer. The idea of constant accretion in this system, despite the lack of X-ray emission, is backed up by the relatively constant spin-up of the neutron star throughout the entire *RXTE* monitoring campaign. Since the lack of pulsations at such a high flux is improbable for this spin period, the most likely explanation from the data presented here is that either a nearby absorbing material sometimes acts to prevent the X-ray emission reaching the observer, or a change in the geometry of the emission column or magnetic field of the neutron star directs the emission away from us at certain times. The other possible scenario is that a near-circular orbit barely brings the neutron star into contact with the disc, causing a weak interaction every periastron passage. This could spin the neutron star up and cause a spike in the optical light curve without resulting in a detectable X-ray outburst. At the times when an outburst is seen, the accretion rate is likely to have increased, though with a very stable disc it is unclear what could cause the system to outburst. Determining the orbit of this system would provide a huge step to understanding its strange behaviour, though this would have to be done through optical radial velocity work, as the X-ray outbursts are not suitable for such an analysis.

ACKNOWLEDGEMENTS

LJT is supported by a Mayflower scholarship from the University of Southampton. MPES is funded through the Claude Leon Foun-

ation and the NRF of South Africa. We are grateful to the staff at SAAO, and Tetsuya Nagata, for support during the 1.9-m and IRSF telescope runs. This work is based on observations made with ESO Telescopes at the La Silla Observatory under programme ID 079.D-0371(A). ABH acknowledges that this research was supported by a Marie Curie International Outgoing Fellowship within the 7th European Community Framework Programme (FP7/2007–2013) under grant agreement no. 275861. We thank Helen Klus for her help with some of the data analysis and the referee for their comments on which this paper has benefitted.

REFERENCES

- Antoniu V., Hatzidimitriou D., Zezas A., Reig P., 2009, *ApJ*, 707, 1080
 Aschenbach B., 2002, *Proc. SPIE*, 4496, 8
 Coe M. J., Edge W. R. T., Galache J. L., McBride V. A., 2005, *MNRAS*, 356, 502
 Corbet R. H. D., 1996, *ApJ*, 457, L31
 Corbet R., Marshall F. E., Lochner J. C., Ozaki M., Ueda Y., 1998, *IAU Circ.*, 6803
 Corbet R. H. D., Bartlett E. S., Coe M. J., McBride V. A., Townsend L. J., Schurch M. P. E., Marshall F. E., 2010, *Astron. Telegram* 2813
 Diaz J., Bekki K., 2011, *MNRAS*, 413, 2015
 Dickey J. M., Lockman F. J., 1990, *ARA&A*, 28, 215
 Dray L. M., 2006, *MNRAS*, 370, 2079
 Evans C. J., Howarth I. D., Irwin M. J., Burnley A. W., Harries T. J., 2004, *MNRAS*, 353, 601
 Galache J. L., Corbet R. H. D., Coe M. J., Laycock S., Schurch M. P. E., Markwardt C., Marshall F. E., Lochner J., 2008, *ApJS*, 177, 189
 Gardiner L. T., Noguchi M., 1996, *MNRAS*, 278, 191
 Ghosh P., Lamb F. K., 1979, *ApJ*, 234, 296
 Goldwurm A. et al., 2003, *A&A*, 411, 223
 Haberl F., Sasaki M., 2000, *A&A*, 359, 573
 Haberl F., Eger P., Pietsch W., 2008, *A&A*, 489, 327
 Harries T. J., Hilditch R. W., Howarth I. D., 2003, *MNRAS*, 339, 157
 Hilditch R. W., Howarth I. D., Harries T. J., 2005, *MNRAS*, 357, 304
 Hill A. B., Dubois R., Torres D. F., Fermi LAT Collaboration, 2011, *High-Energy Emission from Pulsars and their Systems*. Springer-Verlag, Berlin, 2011, p. 498
 Horne J. H., Baliunas S. L., 1986, *ApJ*, 302, 757
 Jahoda K., Markwardt C. B., Radeva Y., Rots A. H., Stark M. J., Swank J. H., Strohmayer T. E., Zhang W., 2006, *ApJS*, 163, 401
 Kato D. et al., 2007, *PASJ*, 59, 615
 Kawano H., Higuchi T., 1995, *Geophys. Res. Lett.*, 22, 307
 Lebrun F. et al., 2003, *A&A*, 411, 141
 Lennon D. J., 1997, *A&A*, 317, 871
 Lund N. et al., 2003, *A&A*, 411, 231
 McBride V. A., Coe M. J., Negueruela I., Schurch M. P. E., McGowan K. E., 2008, *MNRAS*, 388, 1198
 Marshall F. E., Lochner J. C., Takeshima T., 1997, *IAU Circ.*, 6777, 2
 Meyssonnier N., Azzopardi M., 1993, *A&AS*, 102, 451
 Morgan W. W., Keenan P. C., Kellman E., 1943, *An Atlas of Stellar Spectra, with an Outline of Spectral classification*. Univ. Chicago Press, Chicago
 Nagashima C. et al., 1999, in Nakamoto T., ed., *Star Formation 1999*, Nobeyama Radio Observatory, Japan, p. 397
 Negueruela I., Okazaki A. T., 2000, in Smith M. A., Henrichs H. F., Fabregat J., eds, *ASP Conf. Ser. Vol. 214, IAU Colloq. 175: The Be Phenomenon in Early-Type Stars*. Astron. Soc. Pac., San Francisco, p. 713
 Negueruela I., Okazaki A. T., 2001, *A&A*, 369, 108
 Putman M. E., Staveley-Smith L., Freeman K. C., Gibson B. K., Barnes D. G., 2003, *ApJ*, 586, 170
 Reig P., Fabregat J., Coe M. J., 1997, *A&A*, 322, 193
 Sasaki M., Haberl F., Pietsch W., 2000, *A&AS*, 147, 75
 Scaringi S. et al., 2010, *A&A*, 516, 75
 Schmidtke P. C., Cowley A. P., Levenson L., Sweet K., 2004, *AJ*, 127, 3388

- Sguera V. et al., 2005, *A&A*, 444, 221
Sidoli L., 2011, Invited talk at the 25th Texas Symposium on Relativistic Astrophysics, held in Heidelberg, Germany, on December 6–10, 2010, preprint (arXiv:1103.6174)
Strüder L. et al., 2001, *A&A*, 365, L18
Turner M. J. L. et al., 2001, *A&A*, 365, L27
Ubertini P. et al., 2003, *A&A*, 411, 131
Udalski A., 2008, *Acta Astron.*, 58, 187
- Walborn N. R., Fitzpatrick E. L., 1990, *PASP*, 102, 379
Wegner W., 2006, *MNRAS*, 371, 185
Winkler C. et al., 2003, *A&A*, 411, 1
Yokogawa J., Imanishi K., Tsujimoto M., Koyama K., Nishiuchi M., 2003, *PASJ*, 55, 161

This paper has been typeset from a $\text{\TeX}/\text{\LaTeX}$ file prepared by the author.